

Selective mass enhancement close to the quantum critical point in $\text{BaFe}_2(\text{As}_{1-x}\text{P}_x)_2$

V. Grinenko^{1,2,3}, K. Iida^{2,3}, F. Kurth^{1,2}, D. V. Efremov², S.-L. Drechsler², I. Cherniavskii⁴, I. Morozov^{2,4}, J. Hänisch^{2,5}, T. Förster⁶, C. Tarantini⁷, J. Jaroszynski⁷, B. Maierov⁸, M. Jaime⁸, A. Yamamoto⁹, I. Nakamura³, R. Fujimoto³, T. Hatano³, H. Ikuta³, and R. Hühne²

¹Institute for Solid State Physics, TU Dresden, 01069 Dresden, Germany

²IFW Dresden, Helmholtzstrasse 20, 01069 Dresden, Germany

³Department of Crystalline Materials Science, Graduate School of Engineering, Nagoya University, Furo-cho, Chikusa-ku, Nagoya 464-8603, Japan

⁴Lomonosov Moscow State University, GSP-1, Leninskie Gory, Moscow, 119991, Russian Federation

⁵Karlsruhe Institute of Technology, Institute for Technical Physics, Hermann-von-Helmholtz-Platz 1, 76344 Eggenstein-Leopoldshafen, Germany

⁶Hochfeld-Magnetlabor Dresden (HLD-EMFL), Helmholtz-Zentrum Dresden-Rossendorf, 01314 Dresden, Germany

⁷NHMFL, Florida State University, Tallahassee, FL 32310, USA

⁸MPA-CMMS, Los Alamos National Laboratory, Los Alamos, NM, 87545, USA

⁹Department of Applied Physics, Tokyo University of Agriculture and Technology 2-24-16 Nakacho, Koganei, Tokyo 184-8588, Japan

ABSTRACT

A quantum critical point (QCP) is currently being conjectured for the $\text{BaFe}_2(\text{As}_{1-x}\text{P}_x)_2$ system at the critical value $x_c \approx 0.3$. In the proximity of a QCP, all thermodynamic and transport properties are expected to scale with a single characteristic energy, given by the quantum fluctuations. Such an universal behavior has not, however, been found in the superconducting upper critical field H_{c2} . Here we report H_{c2} -data for epitaxial thin films extracted from the electrical resistance measured in very high magnetic fields up to 67 Tesla. Using a multi-band analysis we find that H_{c2} is sensitive to the QCP, implying a significant charge carrier effective mass enhancement at the doping-induced QCP that is essentially band-dependent. Our results point to two qualitatively different groups of electrons in $\text{BaFe}_2(\text{As}_{1-x}\text{P}_x)_2$. The first one (possibly associated to hot spots or whole Fermi sheets) has a strong mass enhancement at the QCP, and the second one is insensitive to the QCP. The observed duality could also be present in many other quantum critical systems.

Introduction

In most of unconventional superconductors, a quantum critical point (QCP) of charge or spin density wave (CDW/SDW) states lies beneath the superconducting dome.¹⁻⁴ Low-energy quantum fluctuations in the vicinity of a QCP lead to non-Fermi liquid (nFL) behavior in the normal state and a strong enhancement of the effective electron mass (m^*). A good example is given by heavy fermion superconductors. In some of these systems the maximum superconducting transition temperature (T_c) coincides with the position of the expected QCP of the magnetic phase.⁴ The presence of a QCP beneath the superconducting dome is evidenced by a strong enhancement of the superconducting specific heat jump $\Delta C/T_c$ at T_c and the slope of the upper critical field $|H'_{c2}| = |dH_{c2}/dT|$ normalized by the critical temperature in the vicinity of T_c .⁵

In multi-band iron-based superconductors (FBS), the maximum of T_c is usually linked to the expected position of a QCP of the SDW phase.⁶ Evidence for a zero-temperature second order magnetic transition with pronounced quantum fluctuations was found for optimally doped $\text{BaFe}_2(\text{As}_{1-x}\text{P}_x)_2$ by various measurements in the normal state.⁷⁻¹² Therefore, it is considered to be a classical example of unconventional superconductivity emerging in the vicinity of a magnetic state.^{13,14} However, no doping dependence of the scattering rates expected for a QCP scenario was observed in recent angle-resolved photoemission spectroscopy (ARPES) studies.¹⁵ In the superconducting state, a divergent quasiparticle effective mass (m^*) above the QCP of the SDW phase was suggested based on specific heat¹⁶ and penetration depth measurements^{17,18} as well as predicted by theoretical studies.^{19,20} However, H_{c2} at low T and its slope near T_c are insensitive to the QCP.²¹ This behavior is seemingly in contradiction to many other experimental observations. To resolve this puzzle we investigated in detail the temperature dependence of H_{c2} for $\text{BaFe}_2(\text{As}_{1-x}\text{P}_x)_2$ single-crystalline thin films in a wide range of P-doping. The obtained data can

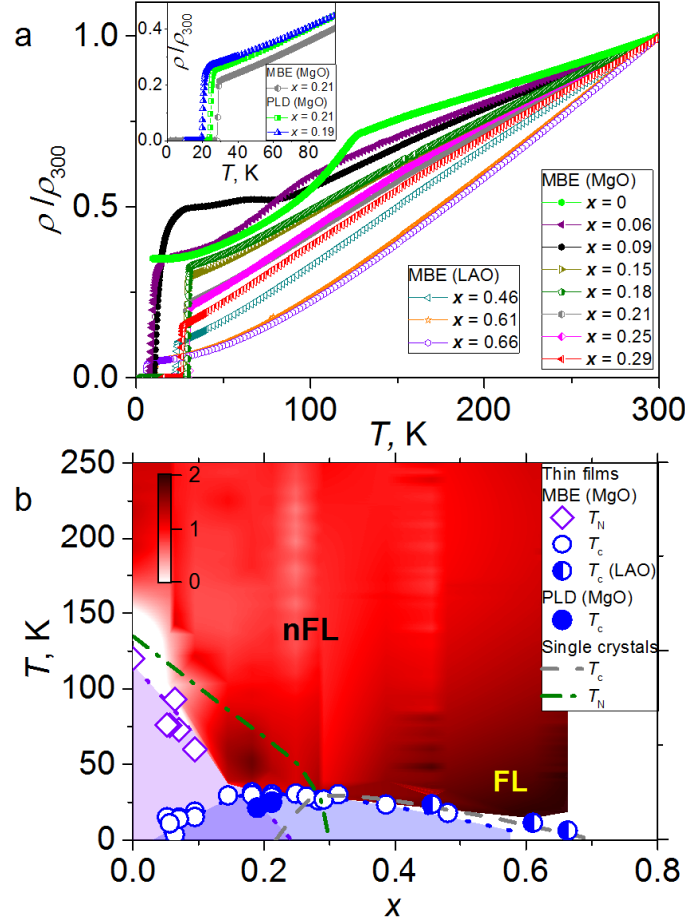


Figure 1. (a) The temperature dependence of the normalized resistivity ρ/ρ_{300K} of $\text{BaFe}_2(\text{As}_{1-x}\text{P}_x)_2$ films prepared by MBE. Closed symbols - underdoped, half closed symbols - optimally doped, and open symbols - overdoped samples. Inset: The normalized resistivity traces for $\text{BaFe}_2(\text{As}_{1-x}\text{P}_x)_2$ thin films with the similar P-doping prepared by PLD and MBE. (b) The phase diagram of $\text{BaFe}_2(\text{As}_{1-x}\text{P}_x)_2$ thin films (symbols). The data of $\text{BaFe}_2(\text{As}_{1-x}\text{P}_x)_2$ single crystals (dashed lines)^{14,25} are also shown for comparison. The whole phase diagram for the thin films prepared on MgO substrates is shifted to lower doping levels compared to that of the single crystals and films prepared on LAO substrates. The shift of the phase diagram is substrate-dependent due to different in-plane strain. The contour plot of the doping and temperature dependence of the exponent n is obtained from the data shown in Fig. 1a and in Ref.²³ assuming $\rho = \rho_0 + AT^n$. The position of the QCP is around $x_c \sim 0.25$ for the films prepared on MgO substrates. The positions of the QCP for the single crystals and films prepared on LAO substrates are nearly coincides at $x_c \sim 0.30$. For further details see text. The dotted lines are guides to the eyes.

be described in an effective two-band model with qualitatively different doping dependences of the Fermi velocities (v_F). Namely, v_{F1} is indeed nearly featureless across the QCP implying a doping independent m_1^* . On the other hand, v_{F2} is strongly doping-dependent, in accord with the almost divergent logarithmic enhancement of m_2^* observed in many other experiments.

Results

Electronic phase diagram of $\text{BaFe}_2(\text{As}_{1-x}\text{P}_x)_2$

$\text{BaFe}_2(\text{As}_{1-x}\text{P}_x)_2$ epitaxial thin films were grown by molecular beam epitaxy (MBE).^{22,23} The investigated MBE thin films have high crystalline quality with T_c values above 30 K at optimal doping level. Some of the films were prepared by pulsed laser deposition (PLD). The PLD films have slightly reduced T_c at similar doping levels compared to the films prepared by MBE as shown in inset of Fig. 1a. This result is consistent with previous studies.²⁴ To construct the phase diagram of our thin films, we analyzed the temperature dependence of the resistivity for various doping levels shown in Fig. 1a. The phase diagrams of the $\text{BaFe}_2(\text{As}_{1-x}\text{P}_x)_2$ thin films and single crystals^{14,25} are shown in Fig. 1b. The whole phase diagram for the thin films prepared on MgO substrates is shifted to lower doping levels compared to that of the single crystals. The shift of the phase diagram, as it was shown in previous studies, is substrate-dependent due to different in-plane strain.^{22,23,26–28} In particular, the in-plane tensile strain for the films grown on MgO modifies slightly the position of the bands resulting in the observed difference between the phase diagrams of thin films and single crystals.²⁸ On the other hand, the amount of strain for the films grown on LaAlO_3 (LAO) is negligibly small resulting in the same phase diagram as for single crystals.²³

We assumed that the temperature dependences of the resistivity (Fig. 1a) can be described by $\rho = \rho_0 + AT^n$ in the normal state above the superconducting and magnetic transition temperatures. This general expression has been frequently employed in the quantum critical region, where $n = 1$ at the QCP and $n = 2$ in a Fermi liquid (FL) state.^{8,14} The contour plot in Fig. 1b illustrates the temperature and doping dependences of the exponent $n = \frac{T d^2 \rho / dT^2}{d\rho / dT} + 1$, as calculated using experimental temperature dependences of the resistivity. In this analysis we exclude the data close to the SDW transition, where $d\rho / dT \lesssim 0$ (white region in Fig. 1b). The region in the phase diagram with nFL behavior is similar to the single crystals: the exponent n shows a V-shape; however, it shifts to lower doping level. This allows to estimate the critical doping level for thin films on MgO substrates as $x_c \approx 0.25 \pm 0.03$, which is slightly lower than $x_c \approx 0.3$ reported for single crystals.¹⁴ For the films prepared on LAO substrate we assumed that the position of the QCP coincides with the QCP position for the single crystals due to close similarity between their phase diagrams as discussed above.

Upper critical field

The temperature dependences of H_{c2} for $\text{BaFe}_2(\text{As}_{1-x}\text{P}_x)_2$ thin films with various doping levels for fields parallel to the c -axis are shown in Fig. 2. The temperature dependence of H_{c2} is strongly affected by the amount of doping. To compare the data of samples with different doping levels, we plot the reduced field $h_{c2} = \frac{H_{c2}}{-H'_{c2}T_c}$ versus the reduced temperature $t = T/T_c$ in Fig. 2b, where H'_{c2} is the extrapolated slope of H_{c2} at T_c . For the strongly overdoped, and slightly underdoped samples, $0.15 < x < 0.21$, the experimental h_{c2} data are close to the prediction of the single-band Werthamer-Helfand-Hohenberg (WHH) model which includes only the orbital pair-breaking effect.²⁹ For other doping levels, the experimental h_{c2} data deviate from the single band fit. The doping dependence of $h_{c2}(0)$ extrapolated to zero temperature is shown in the inset of Fig. 2b. The $h_{c2}(0)$ values exhibit a broad maximum around optimal doping x_c . Additionally, $h_{c2}(0)$ is strongly enhanced in the coexistence state between SC and magnetism, where $T_N > T_c$.

The doping evolution of the temperature dependences of H_{c2} can be described by the two-band model for a clean superconductor as proposed by Gurevich^{30,31} assuming a dominant interband coupling $\lambda_{12}\lambda_{21} \gg \lambda_{11}\lambda_{22}$ as expected for s_{\pm} superconductors. The expression for $B \parallel c$ is given in the Supplementary material Eq. S1. A small value of the intraband couplings $\lambda_{11} = \lambda_{22} \sim 0.1$ affects the resulting Fermi velocities within 10 %, only around optimal doping (see Fig. S7) and it has a negligible effect for overdoped samples. Therefore, to reduce the number of fitting parameters, we adopted zero intraband $\lambda_{11} = \lambda_{22} = 0$ pairing constants. In this case, the superconducting transition temperature is related to the coupling constants by $T_c = 1.14\Omega_{\text{sf}}e^{(-1/\lambda_{12}\lambda_{21})}$. We considered two different values of the characteristic spin fluctuation energy Ω_{sf} , 100 K and 62 K, in order to take into account a possible softening of the spin fluctuations spectrum at the QCP. We assumed also that the paramagnetic pair breaking is negligibly weak, $\alpha_M \ll 1$, as suggested by the small electronic susceptibility of $\text{BaFe}_2(\text{As}_{1-x}\text{P}_x)_2$, where the Maki parameter $\alpha_M = 2^{1/2}H_{c2}^{\text{orb}}/H_p$, defined by a ratio between orbital critical field H_{c2}^{orb} and Pauli limiting field H_p , quantifies the strength of the paramagnetic pair breaking (see also the Supplementary material). This assumption is consistent with a relatively small Knight shift of $\text{BaFe}_2(\text{As}_{1-x}\text{P}_x)_2$.¹² The result of the fit is shown in Fig. 2, and the obtained fitting parameters are given in the Supplementary tables (Tabs. S1 and S2).

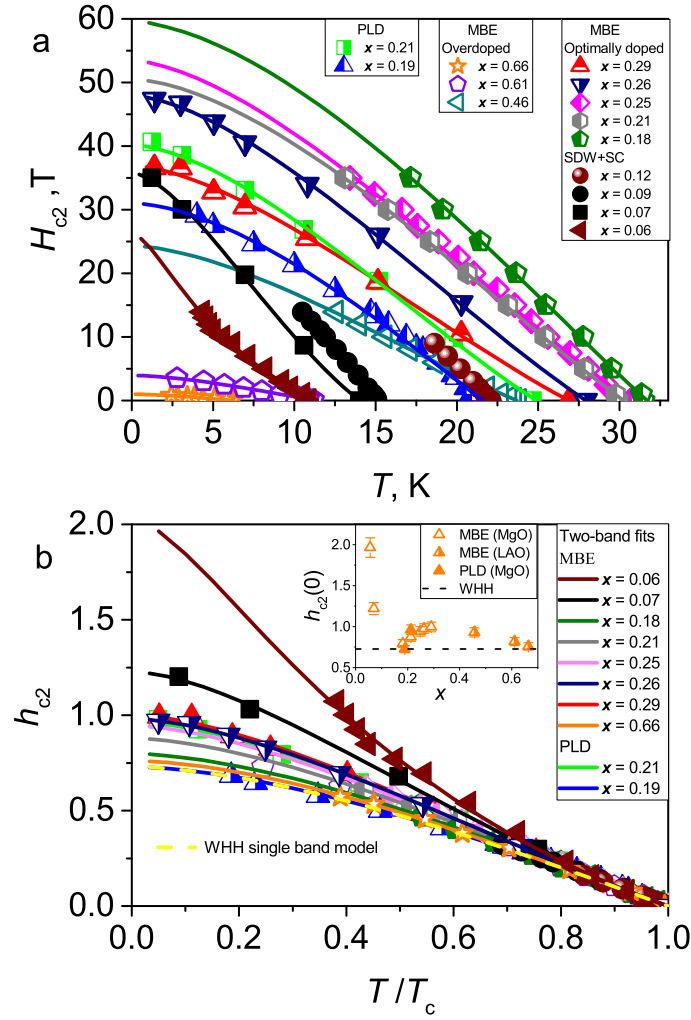


Figure 2. (a) Temperature dependences of the upper critical field H_{c2} of $\text{BaFe}_2(\text{As}_{1-x}\text{P}_x)_2$ thin films with various doping levels for the magnetic field applied along the c -axis. Closed symbols - underdoped, half-open symbols - optimally doped, and open symbols - overdoped samples, solid lines - two-band fits. (b) The reduced field $h_{c2} = \frac{H_{c2}}{-H_{c2}^0 T_c}$ as a function of T/T_c for the data shown in Fig. 2a, solid lines - two-band fits (the same as in Fig. 2a), dashed line - single-band WHH model. The inset shows the doping dependence of the $h_{c2}(0)$ values extrapolated to $T = 0$. The deviation of the experimental data from the single-band curve indicates a relevance of multi-band effects for the temperature dependencies of H_{c2} . This deviation is doping dependent as shown in the inset and it can be described by a two-band model for a clean superconductor with a dominate interband coupling. For further details see text.

Discussion

The doping dependencies of $|H'_{c2}/T_c|^{0.5}$ extrapolated to T_c , and the $H_{c2}(0)^{0.5}/T_c$ extrapolated to $T = 0$ are shown in Fig. 3a. According to the BCS theory for clean superconductors, these values are proportional to the quasiparticle effective mass (m^*). As it was pointed out in Ref.²¹, $|H'_{c2}/T_c|^{0.5}$ should have a peak-like maximum at the QCP of the SDW phase since m^* is strongly enhanced near optimal doping on the whole Fermi surface according to various experimental data.^{7,16,17} However, this is not the case: $|H'_{c2}/T_c|^{0.5}$ and $H_{c2}(0)^{0.5}/T_c$ are nearly featureless at optimal doping ($x_c \sim 0.25$) in accord with Ref.²¹. Both the single crystals and our MBE films have high T_c values of about 30 K at optimal doping indicating similar low impurity scattering rates. The slightly higher $|H'_{c2}/T_c|^{0.5}$ values of the single crystals compared to those of the MBE films are probably related to the different experimental methods used for the evaluation of H_{c2} . Also, H_{c2} of the PLD films follows the same trend in spite of a lower T_c and residual resistivity ratio (inset of Fig. 1a) as compared to those of the MBE films. Therefore, we believe that the observed doping dependence of H_{c2} is not affected essentially by impurity scattering rates and related instead mainly to the changes of v_F and the coupling constants.

H_{c2} of multi-band unconventional s -wave superconductors with dominant interband coupling is limited by the largest v_F in the usually considered pronounced s_{\pm} -regime.^{30,31} Therefore, in the case of a strong v_F asymmetry between different bands, the larger Fermi velocity (v_{F1} in our notation) dominates H_{c2} around optimal doping. In this case one can write $(H'_{c2}/T_c)^{0.5} \propto H_{c2}(0)^{0.5}/T_c \propto v_{F1}^{-1} \propto m_1^*$. This explains the observed weak doping dependence of these quantities (Fig. 3). The obtained doping dependencies of the (normalized reciprocal) v_{F1} and v_{F2} are shown in Fig. 3b. The $1/v_{F1}$ values are indeed smaller than $1/v_{F2}$ and show a weaker doping dependence. In contrast, $1/v_{F2}$ is strongly enhanced around optimal doping. The Ω_{sf} value affects the Fermi velocities quantitatively but their qualitative doping dependence is conserved. The corresponding normalized effective mass m^*/m_b obtained from the de Haas-van Alphen (dHvA) experiments^{7,16} follows the same trend if the small shift of the QCP along the doping axis ($\Delta x = -0.05$) due to the strain is taken into account (see Fig. 1b), where m_b is the quasiparticle mass taken from the band structure calculations. The logarithmic divergence at $x_c = 0.25$ is an indication for the reduction of v_{F2} caused by the quantum fluctuations associated with a QCP of the SDW phase.^{8,16} A strong reduction of v_{F2} is observed also at $x < 0.15$ which roughly corresponds to the doping level where $T_N > T_c$ (Fig. 1b, see also Tabs. S1 and S2 in the Supplementary material). This behavior may be associated with the reconstruction of the Fermi surface due to the presence of the coexisting SDW phase.^{15,32,33}

Some of the multi-band heavy fermion superconductors show a similar behavior around the magnetic QCP as compared to the $\text{BaFe}_2(\text{As}_{1-x}\text{P}_x)_2$ system. The measured enhancement of the effective mass depends also essentially on the experimental method.³⁴ Also, a seemingly conflicting behavior between the dHvA, ARPES and transport data was discussed for cuprate superconductors around optimal hole doping.³⁵ It was proposed that for the suggested nodal electron pocket induced by bidirectional charge order in high fields, the mass enhancement is very anisotropic around the small Fermi surface. It was argued that the corners of that pocket exhibit a large enhancement without any enhancement along the diagonal nodal direction. Such an angle-dependent mass enhancement is interpreted as a destruction of the Landau quasiparticles at 'hot spots' on the large Fermi surface at a proximate QCP. Moreover, another recent theoretical work questioned the paradigm of the universal nFL behavior at a QCP.³⁶ It was shown that at the nematic QCP the thermodynamics may remain of FL type, while, depending on the Fermi surface geometry, either the entire Fermi surface stays cold, or at most there are 'hot spots'. Therefore, one may speculate that the complex behavior observed in FBS and in particular for $\text{BaFe}_2(\text{As}_{1-x}\text{P}_x)_2$ can be related to the superposition of *two distinct* QCPs associated with the SDW phase and the nematic order.³⁷ The evidence for two distinct QCPs was indeed reported for the $\text{Ba}(\text{Fe}_{1-x}\text{Ni}_x)_2\text{As}_2$ system.³⁸ Recently, a band-dependent mass enhancement toward the QCP was suggested from the high-field specific heat measurements of overdoped $\text{BaFe}_2(\text{As}_{1-x}\text{P}_x)_2$ single crystals.³⁹ Thus far, the available experimental data emphasize the relevance of multi-band effects for a proper and complete understanding of the quantum criticality of $\text{BaFe}_2(\text{As}_{1-x}\text{P}_x)_2$ and related systems. Further theoretical and experimental investigations would be helpful to develop a microscopic scenario of the QCP for the title compound and other multi-band systems.

Methods

Samples

$\text{BaFe}_2(\text{As}_{1-x}\text{P}_x)_2$ single crystalline thin films with various P doping levels x were grown by MBE with a background pressure of the order of 10^{-7} Pa. All elements were supplied from solid sources charged in Knudsen cells. Pure elements were used as sources for Ba, Fe, and As. The P_2 flux was supplied from a GaP decomposition source where Ga was removed by two trapping caps placed on the crucible. The details of the sample preparation are given in Refs.^{22,23}. Some of the films on MgO (100) substrate were prepared by PLD with a KrF excimer laser (248 nm). In this case, we used polycrystalline $\text{BaFe}_2(\text{As}_{1-x}\text{P}_x)_2$ as the PLD target material. The preparation process took place in an ultra-high vacuum chamber with a similar base pressure of 10^{-7} Pa. Before the deposition, the substrate was heated to 850 °C. Then the $\text{BaFe}_2(\text{As}_{1-x}\text{P}_x)_2$ layer was grown with a laser repetition rate of 3 Hz. The layer thickness was adjusted via the pulse number at constant laser energy.

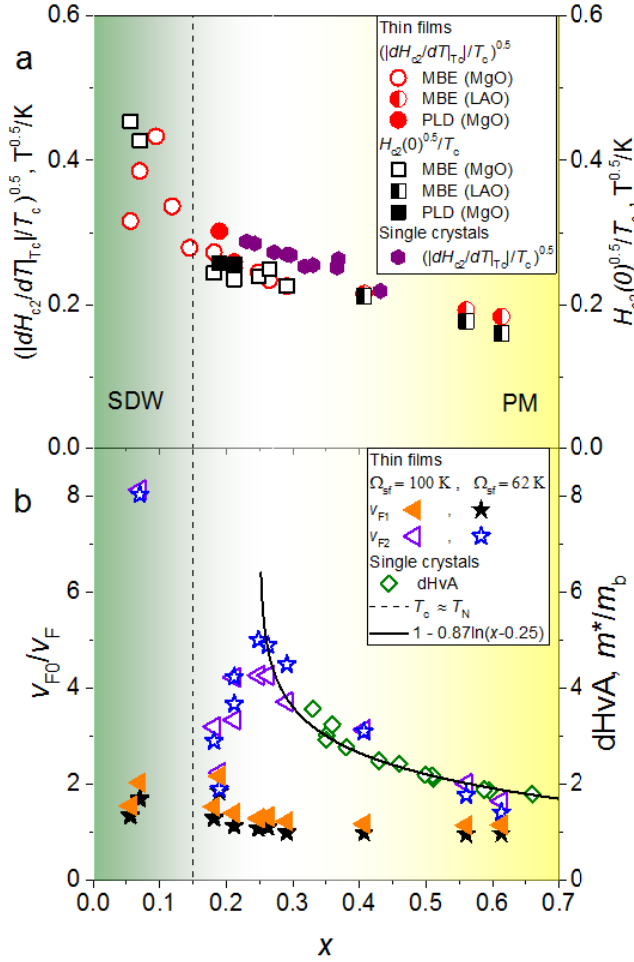


Figure 3. (a, left axis) The normalized slope of the upper critical field $(|H'_{c2}|/T_c)^{0.5}$ at T_c and (a, right axis) the normalized upper critical field $(H_{c2}(0))^{0.5}/T_c$ extrapolated to $T = 0$ using the fits shown in Fig. 2 versus the P-doping level x . Both these quantities are related to the charge carrier effective mass m^* as discussed in the text. The single crystalline data are taken from Ref. 21. (b, left axis) The inversed normalized Fermi velocities v_{F0}/v_{F1} and v_{F0}/v_{F2} in a two-band model are obtained from the fits shown in Fig. 2. (b, right axis) The normalized effective quasiparticle mass m^*/m_b obtained from the dHvA data.^{7,16} The v_{F0} values are chosen to fit dHvA data, $v_{F0} = 1.3 \cdot 10^7$ and $1.1 \cdot 10^7$ cm s⁻¹ for $\Omega_{sf} = 100$ K and 62 K, respectively. All the data of the thin films grown on LAO substrate, and single crystalline data are shifted by $\Delta x = -0.05$ to meet the QCP of the thin films grown on MgO substrate according to Fig. 1b. The solid line is a fit to a phenomenological divergence of the effective mass near a QCP $1/v_{F1} \propto m^* \propto 1 + 0.87 \ln(x - x_c)$ Refs. 8,13 with $x_c = 0.25$. The dashed line denotes approximately the P doping value where $T_c = T_N$.

To improve the sample's homogeneity and thickness gradient, the substrate was rotated during the whole deposition process. Phase purity and crystalline quality of the films were examined by X-ray diffraction (XRD). The c -axis lattice parameters were calculated from the XRD data using the Nelson Riley function. It depends linearly on the P-doping (determined by electron probe micro-analysis (EPMA)) for the films grown on the same substrate.²³ In this work, we mainly investigated films prepared on MgO (100) substrate. At high doping levels, also several films on LaAlO₃ (100) substrate have been used. The P-doping levels given in the paper have been determined using the c -axis lattice parameter values according to the data in Ref.²³ as shown in the Supplementary material Fig. S1.

Resistivity measurements

The temperature dependence of the electrical resistivity was measured by a four-contact method in a Quantum Design physical property measurement system (PPMS) in magnetic fields up to 14 T. Examples of the temperature dependence of the resistivity in zero and applied magnetic fields are shown in Supplementary material (Figs. S2-S7). The high-field measurements were performed in DC magnetic fields up to 35 T at the National High Magnetic Field Laboratory, Tallahassee, FL, USA. The high-field transport measurements in pulsed magnetic fields up to 67 T were performed at the Dresden High Magnetic Field Laboratory at HZDR and at the National High Magnetic Field Laboratory, Los Alamos, NM, USA. The superconducting transition temperature T_c , as given in the paper, was determined using $T_{c,90}$ as shown in the Supplementary material (Figs. S6 and S7). Other criteria, such as 50% of the normal state resistance, yield qualitatively the same temperature dependence of H_{c2} . The SDW transition temperature T_N was defined as the peak position of the temperature derivative of the resistivity curves in analogy to the procedure applied for bulk single crystals⁴⁰, see Supplementary material Fig. S2.

The measurements were performed in magnetic fields applied along the crystallographic c -axis of the films, which coincides with the normal direction of the films surface. Therefore, the H_{c2} data presented in the paper depend on the in-plane coherence length ξ_{ab} only, which is unaffected by the film thickness $D_{\text{film}} \sim 100$ nm. Additionally, $\xi_c > d/2$ is satisfied for all doping levels, where d is the spacing between the neighboring FeAs layers. The estimates given in the Supplementary material indicate that the fluctuation effects close to T_c can be neglected in our case. We assume that the transition width is related to small inhomogeneities in the P distribution and to a difference between $H_{c2}(T)$ and $H_{\text{irr}}(T)$, where H_{irr} is the irreversibility field. In particular, $H_{\text{irr}}(T)$ is noticeably affected by flux pinning at low temperatures and high magnetic fields. Thus, our consideration of BaFe₂(As_{1-x}P_x)₂ thin films as 3D superconductors and the neglect of 2D corrections and fluctuation effects are indeed justified.

References

1. Scalapino, D. J. A common thread: The pairing interaction for unconventional superconductors. *Rev. Mod. Phys.* **84**, 1383 (2012).
2. Hirschfeld, M. M., P. J. Korshunov & Mazin, I. I. Gap symmetry and structure of Fe-based superconductors. *Rep. Prog. Phys.* **74**, 124508 (2011).
3. Gabovich, A. I., A. M. Voitenko & Ausloos, M. Charge- and spin-density waves in existing superconductors: competition between cooper pairing and peierls or excitonic instabilities. *Phys. Reports* **367**, 583–709 (2002).
4. Gegenwart, Q., P. Si & Steglich, F. Quantum criticality in heavy-fermion metals. *Nat. Phys.* **4**, 186–197 (2008).
5. Bauer, E. *et al.* Pressure-induced superconducting state and effective mass enhancement near the antiferromagnetic quantum critical point of CePt₂In₇. *Phys. Rev. B* **81**, 180507(R) (2010).
6. Johnston, D. C. The puzzle of high temperature superconductivity in layered iron pnictides and chalcogenides. *Adv. Phys.* **59**, 803–1061 (2010).
7. Shishido, H. *et al.* Evolution of the fermi surface of BaFe₂(As_{1-x}P_x)₂ on entering the superconducting dome. *Phys. Rev. Lett.* **104**, 057008 (2010).
8. Analytis, J. G. *et al.* Transport near a quantum critical point in BaFe₂(As_{1-x}P_x)₂. *Nat. Phys.* **3**, 194–197 (2014).
9. Hayes, I. M. *et al.* Scaling between magnetic field and temperature in the high-temperature superconductor BaFe₂(As_{1-x}P_x)₂. *Nat. Phys.* 10.1038/nphys3773 (2016).
10. Nakai, Y. *et al.* Unconventional superconductivity and antiferromagnetic quantum critical behavior in the isovalent-doped BaFe₂(As_{1-x}P_x)₂. *Phys. Rev. Lett.* **105**, 107003 (2010).
11. Iye, T. *et al.* Gradual suppression of antiferromagnetism in BaFe₂(As_{1-x}P_x)₂: Zero-temperature evidence for a quantum critical point. *Phys. Rev. B* **85**, 184505 (2012).
12. Nakai, Y. *et al.* Normal-state spin dynamics in the iron-pnictide superconductors BaFe₂(As_{1-x}P_x)₂ and Ba(FeCo_{1-x})₂As₂ probed with nmr measurements. *Phys. Rev. B* **87**, 174507 (2013).

13. Abrahams, E. & Si, Q. Quantum criticality in the iron pnictides and chalcogenides. *J. Phys.: Condens. Matter* **23**, 223201 (2011).
14. Shibauchi, A., T. Carrington & Matsuda, Y. A quantum critical point lying beneath the superconducting dome in iron pnictides. *Annu. Rev. Condens. Matter Phys.* **5**, 113–135 (2014).
15. Fink, J. *et al.* Non-fermi-liquid scattering rates and anomalous band dispersion in ferropnictides. *Phys. Rev. B* **92**, 201106(R) (2015).
16. Walmsley, P. *et al.* Quasiparticle mass enhancement close to the quantum critical point in $\text{BaFe}_2(\text{As}_{1-x}\text{P}_x)_2$. *Phys. Rev. Lett.* **110**, 257002 (2013).
17. Hashimoto, K. *et al.* A sharp peak of the zero-temperature penetration depth at optimal composition in $\text{BaFe}_2(\text{As}_{1-x}\text{P}_x)_2$. *Sci.* **336**, 1554–1557 (2012).
18. Lamhot, Y. *et al.* Local characterization of superconductivity in $\text{BaFe}_2(\text{As}_{1-x}\text{P}_x)_2$. *Phys. Rev. B* **91**, 060504(R) (2015).
19. Levchenko, A. *et al.* Enhancement of the london penetration depth in pnictides at the onset of spin-density-wave order under superconducting dome. *Phys. Rev. Lett.* **110**, 177003 (2013).
20. Nomoto, T. & Ikeda, H. Effect of magnetic criticality and fermi-surface topology on the magnetic penetration depth. *Phys. Rev. Lett.* **111**, 167001 (2013).
21. Putzke, C. *et al.* Anomalous critical fields in quantum critical superconductors. *Nat. Commun.* **5**, 5679 (2014).
22. Kurth, F. *et al.* Unusually high critical current of clean P-doped BaFe_2As_2 single crystalline thin films. *Appl. Phys. Lett.* **106**, 072602 (2015).
23. Kawaguchi, T. *et al.* The strain effect on the superconducting properties of $\text{BaFe}_2(\text{As,P})_2$ thin films grown by molecular beam epitaxy. *Supercond. Sci. Technol.* **27**, 065005 (2014).
24. Sato, H. *et al.* High critical-current density with less anisotropy in $\text{BaFe}_2(\text{As,P})_2$ epitaxial thin films: Effect of intentionally grown c-axis vortex-pinning centers. *Appl. Phys. Lett.* **104**, 182603 (2014).
25. Kasahara, S. *et al.* Evolution from non-fermi- to fermi-liquid transport via isovalent doping in $\text{BaFe}_2(\text{As}_{1-x}\text{P}_x)_2$ superconductors. *Phys. Rev. B* **81**, 184519 (2010).
26. Iida, K. *et al.* Strong T_c dependence for strained, epitaxial $\text{Ba}(\text{Fe}_{1-x}\text{Co}_x)_2\text{As}_2$ thin films. *Appl. Phys. Lett.* **95**, 192501 (2009).
27. Engelmann, J. *et al.* Strain induced superconductivity in the parent compound BaFe_2As_2 . *Nat. Commun.* **4**, 2877 (2013).
28. Iida, K. *et al.* Hall-plot of the phase diagram for $\text{Ba}(\text{Fe}_{1-x}\text{Co}_x)_2\text{As}_2$. *Sci. Rep.* **6**, 28390 (2016).
29. Werthamer, E., N. R. Helfand & Hohenberg, P. C. Temperature and purity dependence of the superconducting critical field, H_{c2} . III. electron spin and spin-orbit effects. *Phys. Rev.* **147**, 295 (1966).
30. Gurevich, A. Upper critical field and the fulde-ferrel-larkin-ovchinnikov transition in multiband superconductors. *Phys. Rev. B* **82**, 184504 (2010).
31. Gurevich, A. Iron-based superconductors at high magnetic fields. *Rep. Prog. Phys.* **74**, 124501 (2011).
32. Yi, M. *et al.* Electronic reconstruction through the structural and magnetic transitions in detwinned nafeas. *New J. Phys.* **14**, 073019 (2012).
33. Nakashima, Y. *et al.* Fermi-surface reconstruction involving two van hove singularities across the antiferromagnetic transition in BaFe_2As_2 . *Solid State Commun.* **157**, 16–20 (2013).
34. Knebel, G. *et al.* The quantum critical point in cerhins: A resistivity study. *J. Phys. Soc. Jpn.*, **77**, 114704 (2008).
35. Senthil, T. On the mass enhancement near optimal doping in high magnetic fields in the cuprates. *arXiv:1410.2096* (2014).
36. Paul, I. & Garst, M. Lattice effects on nematic quantum criticality in metals. *arXiv:1610.06168* (2016).
37. Chowdhury, D. *et al.* Phase transition beneath the superconducting dome in $\text{BaFe}_2(\text{As}_{1-x}\text{P}_x)_2$. *Phys. Rev. B* **92**, 081113(R) (2015).
38. Zhou, R. *et al.* Quantum criticality in electron-doped $\text{BaFe}_{2-x}\text{Ni}_x\text{As}_2$. *Nat. Comm.* **4**, 2265 (2013).
39. Moir, C. M. *et al.* Mass enhancement in multiple bands approaching optimal doping in a high-temperature superconductor. *arXiv:1608.07510* (2016).
40. Pratt, D. K. *et al.* Coexistence of competing antiferromagnetic and superconducting phases in the underdoped $\text{Ba}(\text{Fe}_{0.953}\text{Co}_{0.047})_2\text{As}_2$ compound using x-ray and neutron scattering techniques. *Phys. Rev. Lett.* **103**, 087001 (2009).

Acknowledgements

This work was supported by DFG (GR 4667/1-1). S.-L.D, D.E., I.C. and I.M. thank the VW-foundation for financial support. D.E. also thanks RSCF-DFG Grant. The work at NHMFL was supported by the National Science Foundation Cooperative Agreement No. DMR-1157490 and the State of Florida. K.I. acknowledges the Open Partnership Joint Projects of JSPS Bilateral Joint Research Projects. We acknowledge the support of the HLD at HZDR, member of the European Magnetic Field Laboratory (EMFL). I.C. and I.M. thank the support RSF, grant No. 16-42-01100 and RFBR grant No. 15-03-99628a. We also, acknowledge fruitful discussions with D. Daghero, T. Terashima and J. Wosnitza. The publication of this article was funded by the Open Access Fund of the Leibniz Association.

Author contributions statement

V.G., K.I. and F.K. designed the study. V.G. analyzed H_{c2} data, and wrote the manuscript. D.V.E. and S.-L.D. provided theoretical support in data analysis. I.C., I.M. and A.Y. prepared the PLD targets. Thin PLD films were prepared by V.G., K.I. and F.K. High-field measurements were performed by J.H., T.F., C.T., J.J., B.M., M.J., F.K., K.I. and V.G. V.G. performed transport measurements at magnetic fields up to 14 T. I.N., R.F., T.H. and H.I. prepared and characterized MBE thin films. K.I., J.H., H.I. and R.H. supervised the project. All authors discussed the results and implications and commented on the manuscript.

Additional information

The authors declare no competing financial interests. Correspondence should be addressed to V.G. (v.grinenko@ifw-dresden.de)

Supplementary materials

In the present Supplementary material we show the doping dependence of the c -axis lattice parameter for $\text{BaFe}_2(\text{As}_{1-x}\text{P}_x)_2$ films grown on MgO and LaAlO_3 (LAO) substrates, the temperature dependences of the electrical resistance in magnetic fields, the criteria used for the determination of the SDW transition temperature T_N and the superconducting critical temperature T_c in static magnetic fields as well as the upper critical field H_{c2} in pulsed magnetic fields. We estimated the fluctuation effect on the superconducting transition width and that on the evaluated values of the slope of the upper critical field. Finally, we provide tables with a list of the fitting parameters described in the main text.

Composition of the films

The P doping level of the thin films given in the main text were calculated using the relation between the c -axis lattice parameter and the P doping obtained in previous studies (Fig. S1).^{S1}

Evaluation of T_N and T_c

The spin density wave transition temperatures T_N of the $\text{BaFe}_2(\text{As}_{1-x}\text{P}_x)_2$ films were defined by a standard procedure developed for single crystals (Fig. S2).^{S2}

The temperature dependencies of the upper critical fields H_{c2} given in the main text were obtained from resistivity measurements in static and pulsed magnetic fields (Figs. S3, S4, and S5).

We present two examples of the H_{c2} temperature dependences defined using different criteria $T_{c,0n}$, $T_{c,90}$, and $T_{c,50}$ as shown in Figs. S6a and S7. In all cases, the different criteria result in a quantitative but not a qualitative change of the H_{c2} dependences (Figs. S6b, and S7b). To exclude possible effects of the irreversibility field H_{irr} on the transition width, in the main text we used $T_{c,90}$ to plot H_{c2} (for discussion see below).

Two-band model for H_{c2}

The doping evolution of the temperature dependencies of H_{c2} was described by the two-band model for a clean superconductor as proposed by Gurevich^{S9,S10}. Its expression for $B \parallel c$ is given by

$$a_1 G_1 + a_2 G_2 + G_1 G_2 = 0, \quad (1)$$

where

$$G_1 = \ln t + 2e^{q^2} \text{Re} \sum_{n=0}^{\infty} \int_0^{\infty} e^{-u^2} \left[\frac{u}{n+1/2} - \frac{t}{\sqrt{b}} \tan^{-1} \left(\frac{u\sqrt{b}}{t(n+1/2) + i\alpha b} \right) \right] du,$$

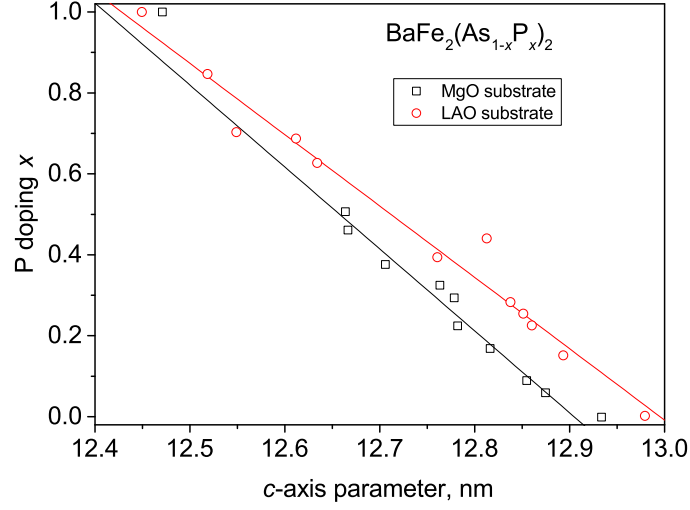


Figure S1. (a) Relation between the c -axis lattice parameter and the P doping level x of $\text{BaFe}_2(\text{As}_{1-x}\text{P}_x)_2$ films grown on MgO and LaAlO_3 (LAO) substrates. The data are taken from previous studies.^{S1}

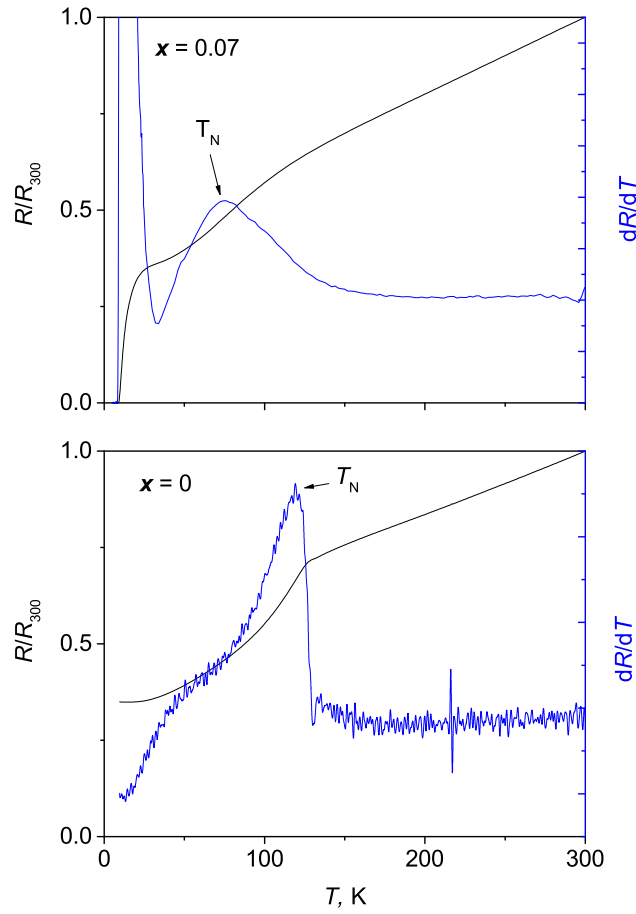


Figure S2. An example of the temperature dependence of the resistance of $\text{BaFe}_2(\text{As}_{1-x}\text{P}_x)_2$ films with SDW transition at low temperatures (left) and its derivative (right). The peak position of the derivative is assigned as T_N . The criterion is based on the comparison between the neutron scattering and transport data for the BaFe_2As_2 system.⁴⁰

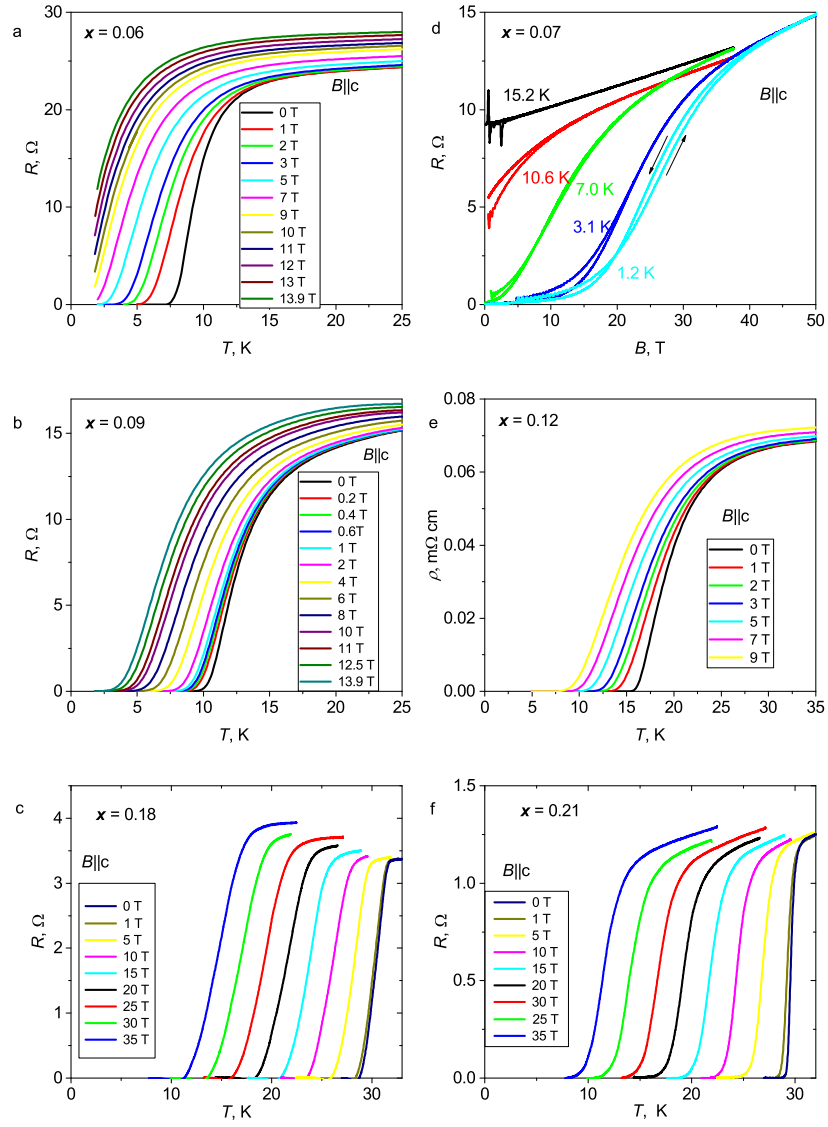


Figure S3. Temperature dependences of the resistance (resistivity if available) of $\text{BaFe}_2(\text{As}_{1-x}\text{P}_x)_2$ films prepared by MBE in static magnetic fields and field dependences of the resistivity in pulsed magnetic fields. The doping levels, fields strength and temperatures are given in the figures too.

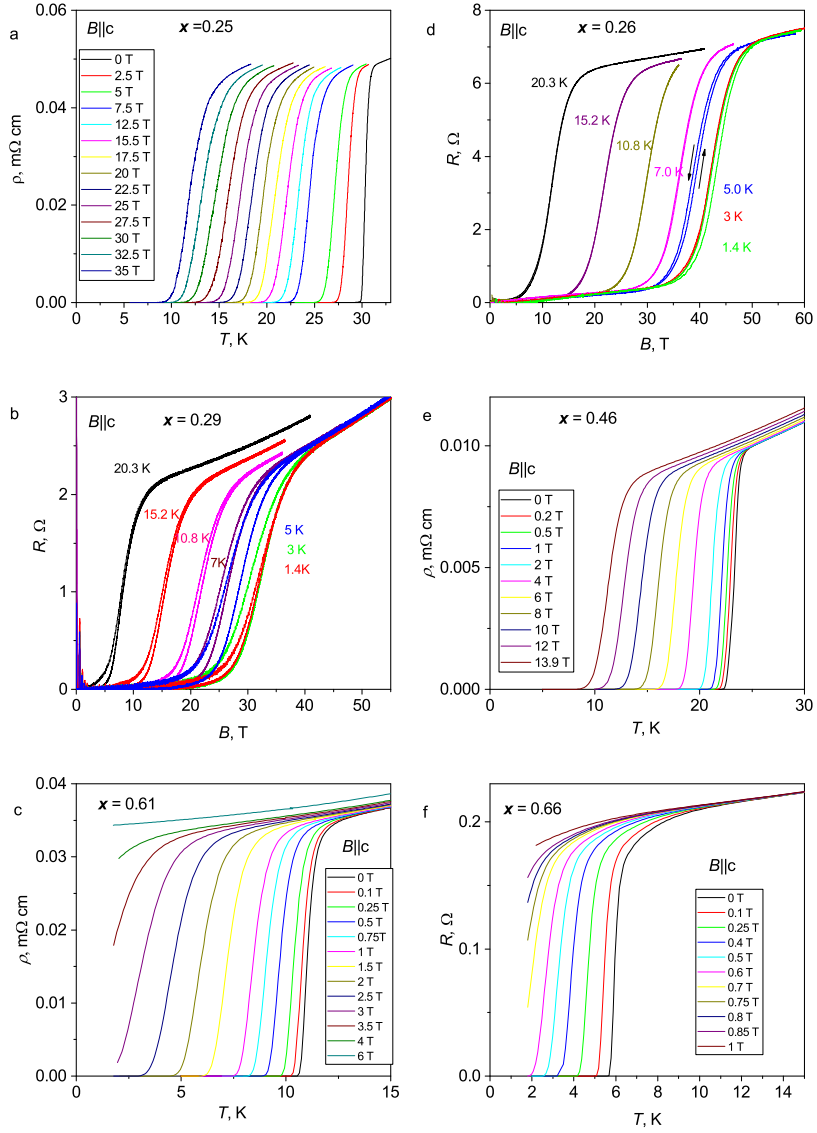


Figure S4. Temperature dependences of the resistance (resistivity if available) of $\text{BaFe}_2(\text{As}_{1-x}\text{P}_x)_2$ films prepared by MBE in static magnetic fields and field dependences of the resistivity in pulsed magnetic fields. The doping levels, fields strength and temperatures are given in the figures too.

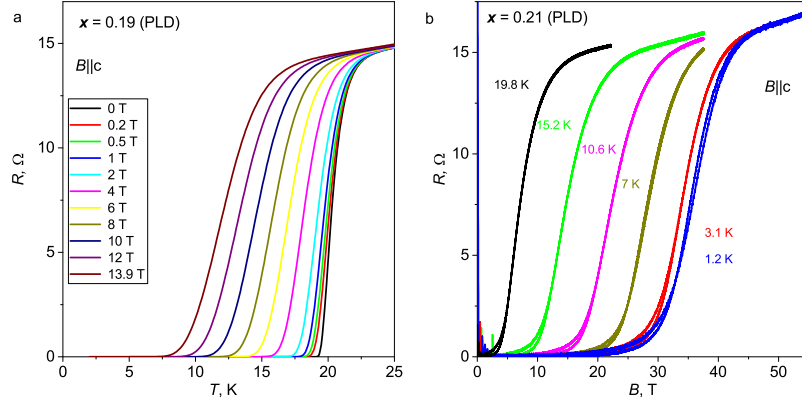


Figure S5. Temperature dependences of the resistance of $\text{BaFe}_2(\text{As}_{1-x}\text{P}_x)_2$ films prepared by PLD in static magnetic fields and field dependences of the resistivity in pulsed magnetic fields. The doping levels, fields strength and temperatures are given in the figures too.

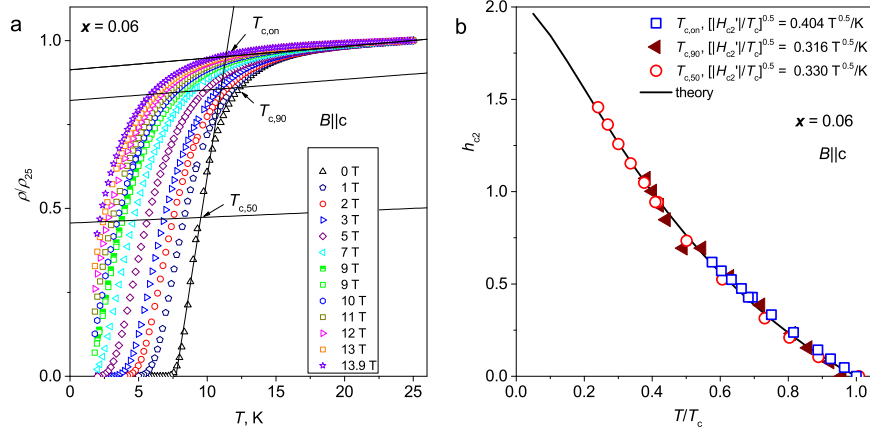


Figure S6. (a) Temperature dependences of the resistance of a $\text{BaFe}_2(\text{As}_{0.94}\text{P}_{0.06})_2$ film prepared by MBE in static magnetic fields. $T_{c,on}$, $T_{c,90}$, and $T_{c,50}$ denote different criteria used to plot the $h_{c2} = \frac{H_{c2}}{-H'_{c2}T_c}$ values versus reduced temperature T/T_c as shown in panel (b).

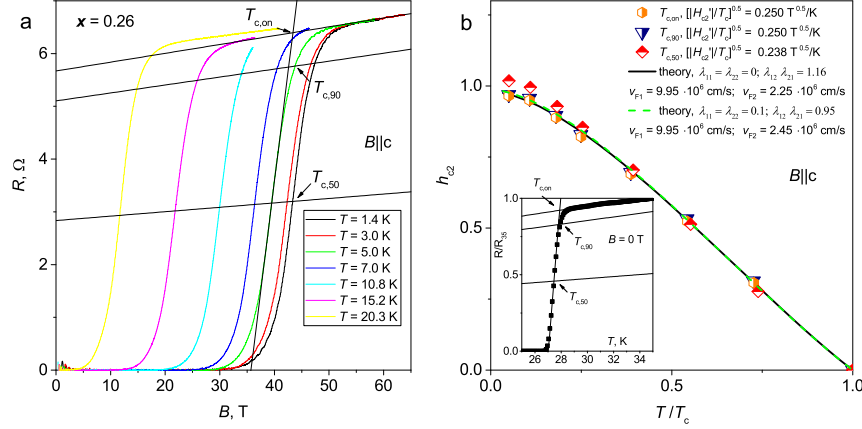


Figure S7. (a) Field dependences of the resistance of a BaFe₂(As_{0.74}P_{0.26})₂ film prepared by MBE (pulsed field measurements). $T_{c,on}$, $T_{c,90}$, and $T_{c,50}$ denote different criteria used to plot the $h_{c2} = \frac{H_{c2}}{-H_{c2}T_c}$ values versus reduced temperature T/T_c as shown in panel (b). The temperature dependence of the normalized resistance R/R_{35} is shown in the inset of panel (b). The fitting curves correspond to two different cases with zero intraband coupling - solid line and non-zero intraband coupling constants - dashed line, where $\Omega_{sf} = 62$ K.

G_2 is obtained by substituting $\sqrt{b} \rightarrow \sqrt{\eta b}$ and $q \rightarrow q\sqrt{s}$ in G_1 ,

$$a_1 = (\lambda_0 + \lambda_-)/2\omega, a_2 = (\lambda_0 - \lambda_-)/2\omega,$$

$$\lambda_- = \lambda_{11} - \lambda_{22}, \lambda_0 = (\lambda_-^2 + 4\lambda_{12}\lambda_{21})^{1/2}, \omega = \lambda_{11}\lambda_{22} - \lambda_{12}\lambda_{21},$$

$$\text{and } b = \frac{\hbar^2 v_{F1}^2 H}{8\pi\phi_0 k_B^2 T_c^2}, q^2 = \frac{Q_z^2 \epsilon_1 \phi_0}{2\pi H}, \alpha = \frac{4\mu\phi_0 T_c}{\hbar^2 v_{F1}^2},$$

where $t = T/T_c$, $\eta = (v_{F2}/v_{F1})^2$, $s = \epsilon_2/\epsilon_1$, v_{Fi} is the in-plane Fermi velocity in band $i = 1, 2$, and $\epsilon_i = m_i^{ab}/m_i^c$ is the mass anisotropy ratio, ϕ_0 is the flux quantum, μ is the magnetic moment of a quasiparticle, λ_{ij} intraband and λ_{ij} , ($j = 1, 2$, and $i \neq j$) interband pairing constants, and $\alpha \approx \alpha_M/1.8$, where the Maki parameter $\alpha_M = 2^{1/2}H_{c2}^{orb}/H_p$ quantifies the strength of the paramagnetic pair breaking. The Fulde-Ferrel-Larkin-Ovchinnikov (FFLO) wave vector \mathbf{Q} is determined by the condition that H_{c2} is at maximum, where Q_z is its projection onto c -axis.

Effect of inhomogeneities and fluctuations on the superconducting transition width

The underdoped films have a relatively broad transition to the superconducting state ΔT_c (see Figs. S3 and S6a). This broadening of the transition can be explained by a small inhomogeneity of the P doping within $\sim 1\%$ together with a strong doping dependency of T_c in the coexistence state between SDW and superconductivity and possible additional broadening in an applied magnetic field due to the irreversibility field H_{irr} . For type-II superconductors in applied magnetic fields the temperature where $R = 0$ depends on the strength of vortex pinning, i.e. the condition where the critical current $I_c = 0$ (for sufficiently small measurement currents) and not by H_{c2} which is related to the condition when the normal vortex cores overlap. Therefore, $R = 0$ corresponds to the irreversibility line H_{irr} rather than to H_{c2} . In general, H_{irr} can differ considerably from H_{c2} .^{S3,S4} Therefore, we avoided to employ this $R = 0$ criterion. We note that the high-field data presented in Ref. S5 reflect the measurements of H_{irr} , which actually differs from H_{c2} .

The effect of superconducting fluctuations plays a secondary role for the ΔT_c values of our thin films. For example, the films with the highest $T_c \sim 30$ K have a transition width of about 1 K, only. Note that, even these transitions width are not yet dominated by fluctuations. Quantitatively, one can estimate the temperature range where fluctuations play a role using the Ginzburg parameter defined in 3D (see also Methods section in the main text) as $\Delta T_c/T_c = Gi \approx 80(T_c/E_F)^4 \sim 10^{-4} - 10^{-5}$.^{S6} Taking $T_c = 30$ K and the largest $E_F \sim 100$ meV in our system according to ARPES data.^{S7} Alternatively, the Gi parameter can be estimated directly from the superconducting parameters: $\Delta T_c/T_c = Gi = (\Gamma k_B T_c / H_{cm}(0)^2 \xi_0^3)^2/2$.^{S3,S8} Taking the experimental values for $T_c = 30$ K, $H_{c2} = 470$ kG, $H_{c1} = 600$ G (field along crystallographic c -axis),^{S5} $\lambda \approx 3 \cdot 10^{-5}$ cm, $\xi_c = [\Phi_0/2\pi H_{c2}]^{0.5} \approx 3 \cdot 10^{-7}$ cm and the anisotropy $\Gamma \sim 2 - 4$, one arrives at the same estimates. However, close to T_c the c -axis coherence length $\xi_c(T)$ diverges as $(1 - T/T_c)^{-0.5}$. Therefore, in close vicinity to T_c , where $\xi_c(T) > D_{film}$, one can consider the films as 2D superconductors, where $D_{film} \approx 100$ nm is the films thickness. For optimally doped films with high H_{c2} values one can estimate that $\xi_c(T) \sim D_{film}$ holds only for a very narrow temperature range of $\Delta T/T_c \approx 0.001$. On the other hand, this range is about 0.5 K for overdoped films with low $T_c \sim 10$ K and small $H_{c2} \sim 10$ kG. However, due to the low

Table 1. The parameters obtained from the fit of H_{c2} temperature dependences shown in Fig. 2 main text. $\Omega_{sf} = 100$ K. The crystallographic c -axis length is given in nm, the Fermi velocities are given in 10^6 cm s^{-1} and the transition temperature is in K.

Substrate/technique	c - axis, Å	P - doping	v_{F1}	v_{F2}	$[\lambda_{12}\lambda_{21}]^{0.5}$	T_c
MgO/MBE	12.877	0.056	8.4	0.65	0.43	11.4
MgO/MBE	12.870	0.070	6.4	1.60	0.48	14.0
MgO/MBE	12.815	0.182	8.5	4.07	0.78	31.7
MgO/MBE	12.800	0.212	9.3	3.90	0.75	30.3
MgO/MBE	12.782	0.248	10.1	3.05	0.76	30.7
MgO/MBE	12.774	0.263	9.8	3.05	0.73	27.9
MgO/MBE	12.761	0.291	10.6	3.50	0.69	26.9
MgO/PLD	12.811	0.190	6.0	5.80	0.70	21.6
MgO/PLD	12.800	0.212	9.3	3.08	0.75	24.9
LAO/MBE	12.736	0.457	11.1	4.15	0.64	23.7
LAO/MBE	12.649	0.610	11.4	6.46	0.44	11.4
LAO/MBE	12.619	0.663	11.3	7.90	0.34	6.3

Table 2. The parameters obtained from the fit of H_{c2} temperature dependences shown in Fig. 2 main text. $\Omega_{sf} = 62$ K. The crystallographic c -axis length is given in nm, the Fermi velocities are given in 10^6 cm s^{-1} and the transition temperature is in K.

Substrate/technique	c - axis, Å	P - doping	v_{F1}	v_{F2}	$[\lambda_{12}\lambda_{21}]^{0.5}$	T_c
MgO/MBE	12.877	0.056	8.20	0.61	0.55	11.4
MgO/MBE	12.870	0.070	6.50	1.37	0.62	14.0
MgO/MBE	12.815	0.182	8.50	3.80	1.25	31.7
MgO/MBE	12.800	0.212	9.70	3.00	1.18	30.3
MgO/MBE	12.782	0.248	10.20	2.20	1.20	30.7
MgO/MBE	12.774	0.263	9.95	2.25	1.08	27.9
MgO/MBE	12.761	0.291	11.05	2.45	1.03	26.9
MgO/PLD	12.811	0.190	6.00	5.80	1.20	21.6
MgO/PLD	12.800	0.212	9.60	2.60	0.96	24.9
LAO/MBE	12.736	0.457	11.30	3.55	0.91	23.7
LAO/MBE	12.649	0.610	11.60	6.23	0.55	11.4
LAO/MBE	12.619	0.663	11.40	7.80	0.41	6.3

T_c , the fluctuation effect is rather weak $\Delta T_c/T_c = Gi \approx (T_c/E_F) \sim 10^{-3}$ even in 2D case.

Finally we list parameters obtained from the fits of H_{c2} temperature dependences shown in the main text (Tabs. 1, and 2), for the case of a zero intraband coupling $\lambda_{11} = \lambda_{22} = 0$.

References

- S1.** T. Kawaguchi, A. Sakagami, Y. Mori, M. Tabuchi, T. Ujihara, Y. Takeda, and H. Ikuta, The strain effect on the superconducting properties of $\text{BaFe}_2(\text{As,P})_2$ thin films grown by molecular beam epitaxy, *Supercond. Sci. Technol.* **27**, 065005 (2014).
- S2.** D. K. Pratt, W. Tian, A. Kreyssig, J. L. Zarestky, S. Nandi, N. Ni, S. L. Bud'ko, P. C. Canfield, A. I. Goldman, and R. J. McQueeney, Coexistence of Competing Antiferromagnetic and Superconducting Phases in the Underdoped $\text{Ba}(\text{Fe}_{0.953}\text{Co}_{0.047})_2\text{As}_2$ Compound Using X-ray and Neutron Scattering Techniques, *Phys. Rev. Lett.* **103**, 087001 (2009).
- S3.** G. Blatter, M. V. Feigel'man, V. B. Geshkenbein, A. I. Larkin, and V. M. Vinokur, Vortices in high-temperature superconductors, *Rev. Mod. Phys.* **66**, 1125 (1994).
- S4.** R. Prozorov, N. Ni, M. A. Tanatar, V. G. Kogan, R. T. Gordon, C. Martin, E. C. Blomberg, P. Pommaphan, J. Q. Yan, S. L. Bud'ko, and P. C. Canfield, Vortex phase diagram of $\text{Ba}(\text{Fe}_{0.93}\text{Co}_{0.07})_2\text{As}_2$ single crystals, *Phys. Rev. B* **78**, 224506 (2008).
- S5.** C. Putzke, P. Walmsley, J. D. Fletcher, L. Malone, D. Vignolles, C. Proust, S. Badoux, P. See, H. E. Beere, D. A. Ritchie, S. Kasahara, Y. Mizukami, T. Shibauchi, Y. Matsuda, A. Carrington, Anomalous critical fields in quantum critical superconductors, *Nat. Commun.* **5**, 5679 (2014).
- S6.** A. Larkin and A. Varlamov, Fluctuation Phenomena in Superconductors, arXiv:cond-mat/0109177.
- S7.** T. Yoshida, I. Nishi, S. Ideta, A. Fujimori, M. Kubota, K. Ono, S. Kasahara, T. Shibauchi, T. Terashima, Y. Matsuda, H. Ikeda, and R. Arita, Two-Dimensional and Three-Dimensional Fermi Surfaces of Superconducting $\text{BaFe}_2(\text{As}_{1-x}\text{P}_x)_2$ and Their Nesting Properties Revealed by Angle-Resolved Photoemission Spectroscopy, *Phys. Rev. Lett.* **106**, 117001 (2011).
- S8.** C. Chaparro, L. Fang, H. Claus, A. Rydh, G. W. Crabtree, V. Stanev, W. K. Kwok, and U. Welp, Doping dependence of the specific heat of single-crystal $\text{BaFe}_2(\text{As}_{1-x}\text{P}_x)_2$, *Phys. Rev. B* **85**, 184525 (2012).
- S9.** A. Gurevich, Upper critical field and the Fulde-Ferrel-Larkin-Ovchinnikov transition in multiband superconductors, *Phys. Rev. B* **82**, 184504 (2010).
- S10.** A. Gurevich, Iron-based superconductors at high magnetic fields, *Rep. Prog. Phys.* **74**, 124501 (2011).